Carotid artery lumen segmentation in 3D free-hand ultrasound images using surface graph cuts

Lorza, Andrés M. Arias; Carvalho, Diego D. B.; Petersen, Jens; Dijk, Anouk C. van; Lugt, Aad van der; Niessen, Wiro J.; Klein, Stefan; de Bruijne, Marleen

Published in:
Medical Image Computing and Computer-Assisted Intervention – MICCAI 2013

DOI:
10.1007/978-3-642-40763-5_67

Publication date:
2013

Document version
Peer-review version

Carotid artery lumen segmentation in 3D free-hand ultrasound images using surface graph cuts

Andrés M. Arias Lorza[1], Diego D. B. Carvalho[1], Jens Petersen[2], Anouk C. van Dijk[3], Aad van der Lugt[3], Wiro J. Niessen[1,4], Stefan Klein[1], and Marleen de Bruijne[1,2]

[1] Departments of Radiology and Medical Informatics, Erasmus MC, The Netherlands
[2] Department of Computer Science, University of Copenhagen, Denmark
[3] Department of Radiology, Erasmus MC, The Netherlands
[4] Faculty of Applied Sciences, Delft University of Technology, The Netherlands

Abstract. We present a new approach for automated segmentation of the carotid lumen bifurcation from 3D free-hand ultrasound using a 3D surface graph cut method. The method requires only the manual selection of single seed points in the internal, external, and common carotid arteries. Subsequently, the centerline between these points is automatically traced, and the optimal lumen surface is found around the centerline using graph cuts. To refine the result, the latter process was iterated. The method was tested on twelve carotid arteries from six subjects including three patients with a moderate carotid artery stenosis. Our method successfully segmented the lumen in all cases. We obtained an average dice overlap with respect to a manual segmentation of 84% for healthy volunteers. For the patient data, we obtained a dice overlap of 66.7%.

1 Introduction

Ultrasound (US) enables low cost non-invasive imaging of the carotid arteries for identifying carotid atherosclerotic plaque [10] and investigating the carotid artery geometry, which are associated with vascular events. Carotid arteries are most frequently imaged using a 2D free-hand US probe; using a tracking device it is possible to compound a series of 2D US images into a 3D volume [6]. Methods for automated lumen segmentation of 3D US data would enable the investigation of carotid artery geometry and the narrowing of the vessel caused by the presence of plaque [1]. However, segmenting the lumen in US is a difficult task, due to image noise, shadows and speckle inside the lumen. Another problem is that in US images the vessel boundary parallel to the US beam is not visible.

Ukwatta et al. [9] proposed a semiautomatic carotid segmentation method on 3D US data using a level set based method. Although their segmentation results are good, this method requires considerable user interaction, as anchor points on transverse slices where the evolving curve must pass through need to be indicated. In addition, they only segment the common carotid artery. A

complete segmentation of the carotid artery based on level sets is proposed by Hossain et al. [7]. However, the user has to initialize boundary points for every slice.

Graph-based methods have been used for vessel segmentation in CTA and MRI obtaining promising results [5, 2]. Surface-based graph methods such as [2] as opposed to voxel based methods [5] make it possible to enforce topology constraints and incorporate a shape prior of the arteries. In this paper we propose a method based on surface graph cuts to segment the complete carotid artery lumen in 3D free-hand US images with minimal user interaction. Following the method presented by Arias et al. [2] for segmenting the carotid artery wall on MRI, we define the graph columns traced from a coarse initial segmentation, which is approximated by a morphological dilation of the lumen centerline. Each graph column is associated with a point on the sought surface and represents the set of possible solutions. As such graph columns do not intersect each other, this enables accurate, non self-intersecting segmentation across high curvature areas such as the carotid bifurcation [2]. Finally, to deal with errors or variability induced by the initialization, this procedure is iterated several times.

2 Method

Centerline Extraction and Initial Segmentation The graph is constructed from a coarse initial segmentation of the carotid vessel lumen, obtained from its centerline. We adapted the US centerline extraction algorithm presented in [4]. This method tracks lumen centerlines in US through ellipse fitting in transversal 2D cross-sections of the artery. The input of the algorithm are three user defined seed points in the lumen, positioned at the beginning of the internal, external and common carotid artery (ICA, ECA and CCA) respectively. From each seed point, rays are traced in all directions of the cross-section checking the pixel intensity at each position. In [4], the ray stops when an intensity above a certain threshold is found, indicating that the border of the vessel has probably been reached. We modified this criterion in order to make it more robust against pixel intensity variations in the lumen. In our approach, directional derivatives are calculated along each ray. The third quartile of all the directional derivatives for all rays is selected as the threshold y_{th}. This is represented as $\sum_{x \leq y_{th}} P_y(x) = 0.75$ where P_y represents the estimated probability distribution of the directional derivatives $y : \Omega_r \rightarrow \mathbb{R}$ given by $y(\boldsymbol{x}) = \frac{\partial I(\boldsymbol{r_x}(t))}{\partial t}$, Ω_r is the set of image positions indicated by the rays in the cross-section, I is the image intensity, and $\boldsymbol{r_x} : \mathbb{R} \rightarrow \mathbb{R}^2$ is the ray trajectory at position $\boldsymbol{x}$. Thereafter, all steps are similar to [4] but considering the directional derivatives instead of the intensities.

The centerline is subsequently smoothed to reduce the influence of noise. The centerline in the CCA is then connected to the centerline in the ICA and the ECA. Finally, the centerline is dilated with a 2mm diameter spherical structuring element to obtain a coarse approximation of the lumen. This rough segmentation acts as an input for the segmentation method.

Graph Construction Based on this initial rough segmentation, a graph is constructed. The surface graph approach proposed in this paper is an adaptation of the method presented by Arias et al. [2]. To construct the graph, first the graph columns have to be traced in the image. Each graph column represents a set of possible solutions for a point in the sought surface. Hereto, the coarse initial segmentation is converted to a surface mesh with vertices V_B at the centers of each face on the surface of the voxelized initial segmentation. These graph vertices V_B represent the starting points of the columns. A schematic of a coarse initial segmentation of the carotid vessel lumen and its mesh conversion is shown in Figures 1(a) and 1(b), respectively.

The graph columns are traced from all V_B, and follow the direction of the flow lines $\boldsymbol{f}\colon \mathbb{R} \to \mathbb{R}^3$ of the gradient vector field obtained by Gaussian smoothing of the initial segmentation $\phi\colon \mathbb{R}^3 \to \mathbb{R}$ [2, 8], this is represented by the equation $\frac{\partial \boldsymbol{f}}{\partial t}(t) = \nabla\phi(\boldsymbol{f}(t))$ with initial value given by $\boldsymbol{f}(0) \in V_B$. An example of a gradient vector field of a smoothed segmentation ϕ is shown in Figure 1(c). The flow lines traced along this gradient vector field, starting from the graph vertices located at the mesh surface are indicated by the red lines in Figure 1(d). From the figure it can be seen that the graph columns defined by flow lines traced along the gradient of ϕ are smooth and non-intersecting. Because in a graph cut method each column is cut once, this results in non-self-intersecting surfaces [8].

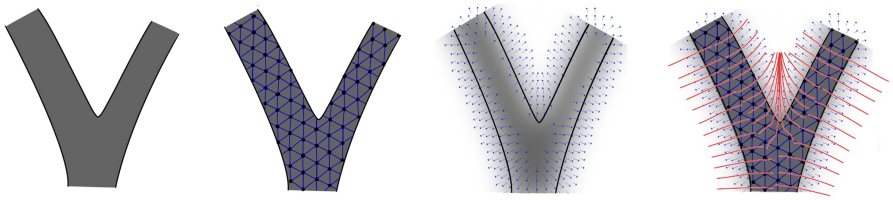

(a) (b) (c) (d)

Fig. 1. Graph columns construction based on flow lines. Graph columns are generated from an initial coarse segmentation as shown in (a). This initial segmentation is converted to a surface mesh, where vertices of the graph columns are at the center of each surface voxel face as depicted in (b) by black dots. Subsequently, the coarse initial segmentation is smoothed and a gradient vector field is computed, see (c). Finally, (d) shows the graph columns represented by red lines which trace this gradient field from the vertices located at the mesh surface.

The remaining column vertices V of the graph, which represent all possible lumen surface segmentation points, are sampled at regular intervals δ along the flow-lines. The length of each column varies, and is defined by the position where the smoothed segmentation ϕ vanishes. Finally, source s and sink t vertices are added to the graph, representing the innermost and outermost vertices respectively. A representation of the vertices in the graph is given in Figure 2(a) by the black dots.

Next, the edges E of the surface graph $G = (V, E)$ need to be defined. The edge set consists of intra-column edges E_{intra} and edges between columns E_{inter} [2, 8]. The intra-column edges are associated to the likelihood that a vertex in a column is part of the lumen surface, while the edges between columns E_{inter} penalize irregularities on the final segmentation, ensuring smooth surfaces. To model this behavior on the surface graph G, the intra-column edges E_{intra} associated with a cost $w \in \mathbb{R}$ are represented by directed edges connecting each vertex to the next vertex in an outward direction in the same column [2]. In addition, the source vertex s is connected to all innermost vertices in the graph, and all outermost vertices are connected to the sink vertex t. A representation of the intra-column edges is provided in Figure 2(a). In our surface graph cut method, the main aim is to find a cut that minimizes the cost of the edges that are being cut. Therefore, the cost w is associated to the inverse of the likelihood that the edge being cut belongs to the sought surface. As in [2], this cost is inversely proportional to the first order derivative along the graph column given by $\frac{\partial I(\boldsymbol{f}(t))}{\partial t}$, where I is the image intensity. This leads to low costs for strong dark to bright transitions that are typically present at the lumen border in US. The true vessel surface may be slightly inward or outward of the image intensity edge position along the column. Therefore, we adjust the position of the lowest value of w along the graph column by adding the second order derivative to the first order derivative. This linear combination is represented by $\alpha \frac{\partial^2 I(\boldsymbol{f}(t))}{\partial t^2}(t) + (1 - |\alpha|) \frac{\partial I(\boldsymbol{f}(t))}{\partial t}$ where α is a parameter representing the contribution of the second order derivative.

In many columns, the position of the lumen boundary will not be clear due to image noise or shadows caused by nearby vessels. To determine the position of the surface in these columns, information from neighboring columns with better contrast in the intensity profiles must be used. Therefore, we add edges between neighboring columns E_{inter}, which linearly penalize jumps between the columns. This way, the local image information associated to the intra-column edges is integrated into a global and smooth segmentation solution. An example of these inter-column edges is depicted in Figure 2(b). In the figure, the edges between columns are depicted by blue arrows. The cut cost associated to the edges between columns is linearly proportional to the number of edges that are being cut.

Finally, a 3D segmentation is obtained by solving the graph cut minimization problem. The vertices located directly inside of the optimal cut represent the sought surface. This minimization is solved by applying a min-cut/max-flow optimization algorithm [3].

Iterative approach Owing to the presence of noise in the image, the extracted initial centerline may present irregularities. Therefore, the coarse initial segmentation may still deviate from the sought lumen surface. Examples of a coarse initial segmentation and the segmentation result after one iteration of the method in image slices are shown in Figure 3. From the figure, we can observe that in some sections the initial segmentation contour is far from the lumen contour.

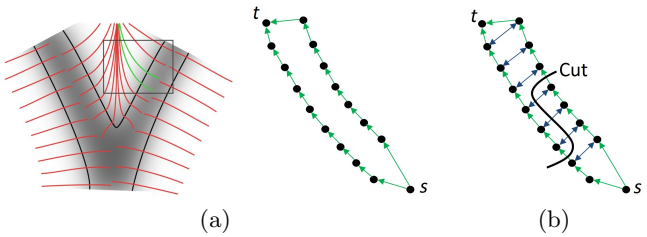

Fig. 2. Description of graph edges. The intra-column edges are depicted by green arrows in (a). The edges between neighbor columns are depicted by blue arrows in (b). Additionally, an example of a graph cut is shown in (b).

With standard column lengths defined by the smoothing scale σ of the initial segmentation, the graph columns may not reach the lumen border resulting in an under segmentation, as is the case in Figure 3. To obtain a correct segmentation in the cases that the initialization is far from the lumen surface, we proposed and evaluated two possible solutions. First, the length of the graph columns can be extended. This is achieved by smoothing the initial segmentation with a higher scale σ, such that the gradient vector field can be traced further, resulting in longer columns. However, these longer columns may intersect edges of other vessels close to the carotid artery possibly resulting in a wrong segmentation. A second option is to apply an iterative approach. Here, the computed segmentation is used as initialization for a new graph. This may work in cases with wrong initialization because if some sections are segmented correctly then the optimal graph cut solution approaches the lumen surface thanks to the smoothness constraint. Example results of the iterative approach are shown in Figure 3, indicating that after every iteration the segmentation results were improved.

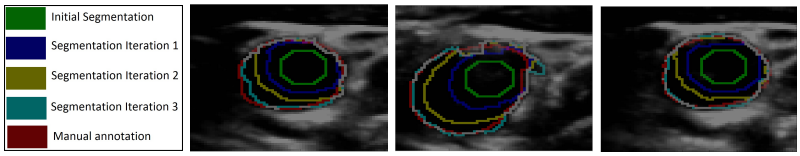

Fig. 3. Segmentation results after several graph cut iterations for different volume slices.

3 Experiments and Results

To validate our method, we segment the carotid lumen in 20 carotid arteries of ten subjects, six healthy volunteers and four patients with a moderate carotid artery stenosis. Each image was acquired using free-hand US on the carotid

section of the neck of the subject. A 3D volumetric representation was obtained with the help of an external software, which correlates the position of a magnetic tracking sensor attached to the US probe and the US machine coordinates [6]. We used a Philips iU-22 US scanner with a L9-3 US probe, acquiring signals of 4cm depth on one patient and of 3cm depth on the remaining subjects. After exporting the data to a volumetric representation, the voxels dimension have 0.16mm^3 for probe depth of 3cm, and 0.21mm^3 for probe depth of 4cm. After, we obtain the centerline with the proposed method, to standardize the data, we cropped centerline points that are outside a 2cm radius from the bifurcation point. The proposed centerline extraction method was able to track the centerline in all cases and estimate the bifurcation point.

All images were manually annotated. The manual segmentation was performed by annotating the lumen at each five to ten 2D slices. Thereafter, the lumen surface was interpolated based on these contours. We used eight carotid arteries from four subjects (three healthy volunteers and one patient) to optimize the parameters of the method: the smoothing scale σ, the weighting parameter α that weights the influence of the first and second order derivatives of the edge cost w, the edge cost between columns p, and the number of iterations N. The sampling vertex distance δ was fixed to the voxel spacing 0.16mm. We performed an exhaustive joint parameter search to find the optimal set of parameters, which optimizes the Dice Segmentation Coefficient (DSC). We obtained the highest DSC using $\sigma = 10$, $\alpha = 0.5$, $p = 10,000$, and $N = 4$. Figure 4 show the effect of variations in the four parameters. The smoothing scale σ has little effect on the end results, while iterating the method clearly improves results.

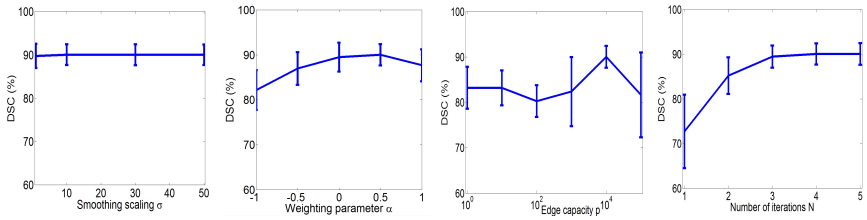

Fig. 4. Effect of the segmentation parameters on segmentation overlap, when varying a single parameter while the other parameters are fixed at their optimum value. The error bars denote the standard deviation. From left to right: the smoothing scaling σ, the weighting parameter α, the edge capacity p, and the number of iterations N.

We tested our method using 3D US images of twelve carotid arteries of three healthy volunteers and three patients. A 3D visualization of the segmentations compared with the manual annotations for a volunteer and a patient are shown in Figure 5(a) and 5(b). A good agreement can be observed from the figures. Figure 5(c) shows the DSC values for the volunteers carotid arteries per iteration. The average DSC after applying four iterations is $84\% \pm 4.9\%$. The DSC values

for the patients arteries are shown in figure 5(d). Here, the obtained average DSC for four iterations is $66.7\% \pm 8.3\%$.

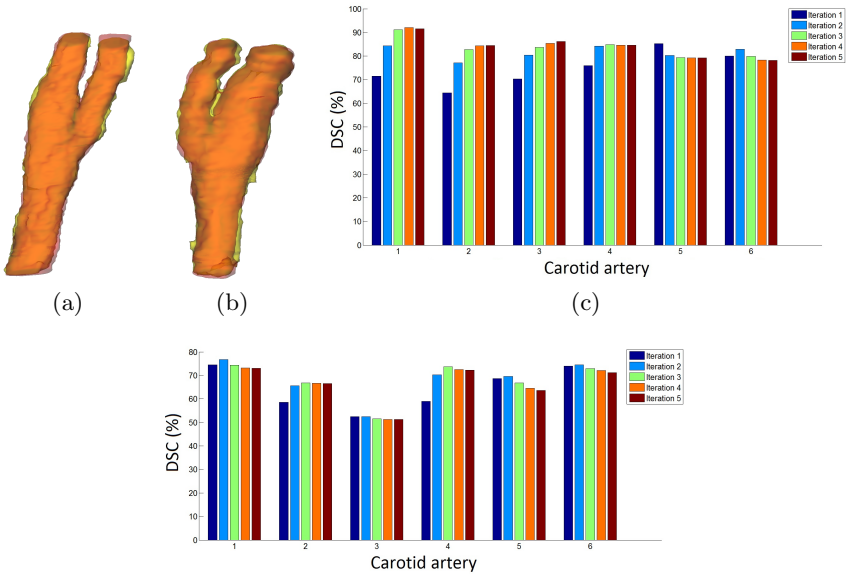

Fig. 5. Segmentation results. Figures (a) and (b) show the manual annotated lumen (red) and the automated segmentation result (yellow) for a volunteer and patient artery respectively. Bar plots with the DSC for volunteer and patient carotid arteries in the testing set per iteration are shown in (c) and (d) respectively.

4 Discussion and Conclusion

In this paper, we propose a new method to segment the carotid artery lumen, including the bifurcation area, in 3D free-hand US images using little user interaction. The obtained results showed good agreement with manual segmentation for healthy arteries, obtaining a DSC of 84% for healthy volunteers. However, the segmentation was less good in patient arteries, with a DSC of an average 66.7%. In this paper, only two diseased arteries were included during the parameter tuning. We expect that including more patient data in the parameter tuning set would lead to a graph model that can describe plaque sections better, resulting in improved performance for these cases.

We proposed an improved centerline extraction method for US image based on [4] which was able to track the centerline and estimate the bifurcation point in all images described in [4], while the method proposed by Carvalho et al. [4] failed in three cases. We also proposed a novel iterative surface graph cut

approach based on [2]. As observed in Figures 5(c) and 5(d) in most of the cases the iterations improve the results.

Compared to the method proposed by Ukwatta et al. [9], who obtained an average DSC of 92%, we obtained lower DSC. However, in contrast to [9], our method can segment the lumen bifurcation, which may be relevant to predict vascular events. In addition, our method requires less user interaction, which makes it more suitable for large scale studies and for use in clinical practice. Hossain et al. [7] reported a method that can segment the complete carotid artery, including the bifurcation area. However, this method also requires substantial user interaction; the user has to locate initialization points on the boundary for every slice. In addition, they reported a processing time of about 40min, whereas our method computes a segmentation in under 3min using an Intel core 2 duo processor with 8 GB of RAM. In summary, the main advantages of our method are the ability to segment the complete carotid artery, fast and with little user interaction.

Acknowledgments. This research was financially supported by the Netherlands Organisation for Scientific Research (NWO).

References

1. Allott et al.: Volumetric assessment of carotid artery bifurcation using freehand-acquired, compound 3d ultrasound. Br J Radiol 72(855), 289–92 (1999)
2. Arias et al.: Carotid artery wall segmentation by coupled surface graph cuts. In: Medical Computer Vision. Recognition Techniques and Applications in Medical Imaging, Lecture Notes in Computer Science, vol. 7766, pp. 38–47. Springer (2013)
3. Boykov, Y., Kolmogorov, V.: An experimental comparison of min-cut/max-flow algorithms for energy minimization in vision. IEEE Transactions on Pattern Analysis and Machine Intelligence 26(9), 1124–1137 (2004)
4. Carvalho et al.: Estimating 3d lumen centerlines of carotid arteries in free-hand acquisition ultrasound. International Journal of Computer Assisted Radiology and Surgery 7, 207–215 (3 2012)
5. Freiman et al.: Vessels-cut: a graph based approach to patient-specific carotid arteries modeling. In: Proceedings of the 2009 international conference on Modelling the Physiological Human. pp. 1–12. 3DPH'09, Springer-Verlag (2009)
6. Gee et al.: Processing and visualizing three-dimensional ultrasound data. Br J Radiol 77(suppl_2), S186–193 (2004)
7. Hossain et al.: Semiautomatic segmentation of atherosclerotic carotid artery lumen using 3d ultrasound imaging. In: Medical Imaging: Computer-Aided Diagnosis. Proceedings of SPIE. (2013)
8. Petersen et al.: Optimal graph based segmentation using flow lines with application to airway wall segmentation. In: Proceedings of the 22nd international conference on Information processing in medical imaging. pp. 49–60. Springer-Verlag (2011)
9. Ukwatta et al.: Three-dimensional semi-automated segmentation of carotid atherosclerosis from three-dimensional ultrasound images. In: Medical Imaging: Computer-Aided Diagnosis. Proceedings of SPIE. (2012)
10. van der Wal, A.C., Becker, A.E.: Atherosclerotic plaque rupture–pathologic basis of plaque stability and instability. Cardiovascular research 41(2), 334–344 (Feb 1999)